

# Exploration of Phaeanthine: A Bisbenzylisoquinoline Alkaloid Induces Anticancer Effect in Cervical Cancer Cells Involving Mitochondria-Mediated Apoptosis

Alisha Valsan, Murugan Thulasi Meenu, Vishnu Priya Murali, Beutline Malgija, Anuja Gracy Joseph, Prakasan Nisha, Kokkuvayil Vasu Radhakrishnan,\* and Kaustabh Kumar Maiti\*



Cite This: *ACS Omega* 2023, 8, 14799–14813



Read Online

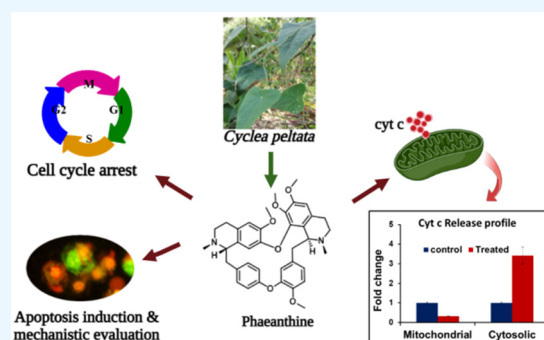
ACCESS |

Metrics & More

Article Recommendations

Supporting Information

**ABSTRACT:** Natural-product-based pharmacophores possess considerably more structural diversity, attractive physicochemical features, and relatively less toxicity than synthesized drug entities. In this context, our studies on phaeanthine, a bisbenzylisoquinoline alkaloid isolated from the rhizomes of *Cyclea peltata* (Lam) Hook.f & Thoms., showed selective cytotoxicity toward cervical cancer cells (HeLa) with an  $IC_{50}$  of  $8.11 \pm 0.04 \mu\text{M}$ . Subsequent investigation with in silico molecular docking of phaeanthine displayed preferential binding to the antiapoptotic protein Akt as reflected by a docking score of  $-5.023$ . Interestingly, the follow-up in vitro assessment of the compound correlated with mitochondria-mediated apoptosis specifically by downregulating the expression of Akt and p-Akt, including other antiapoptotic proteins Mcl-1, IGF-2, and XIAP. In the complementary in vitro assessment, mitochondrial membrane polarization and dynamics of intercellular cytochrome *c* validated the intrinsic mechanism of the apoptotic phenomenon. To the best of our knowledge, this is the first comprehensive anticancer profiling study of phaeanthine against HeLa cells.



reproductive system and for treating many female reproductive disorders.<sup>2,3</sup> The plant enables excess water stagnation with uterine tumors, ovarian cysts, and leucorrhea to decrease.<sup>2</sup> The plant is also traditionally used by tribal communities in India to treat diarrhea, wounds, and certain skin diseases.<sup>4–6</sup> The plant is known to possess many pharmacological properties, including antidiabetic, anticancer potential at an extract level,<sup>7,8</sup> nephroprotective activity,<sup>9</sup> hepatoprotective potential,<sup>10</sup> antibacterial activity,<sup>11,12</sup> gastric antisecretory, and antiulcer property.<sup>13</sup> Additionally, *C. peltata* root extract is effective in neutralizing the venom of *Naja naja*<sup>14</sup> and also shows significant antipyretic and analgesic activity,<sup>15</sup> and the ethyl acetate extract is shown to have anti-inflammatory potential. In Swiss albino rats, the methanolic extract of the plant reduced DAL-induced tumor development.<sup>8</sup> So, based on the available literature, it is clear that the plant possesses antitumor potential, but an in-depth evaluation of the key phytomolecule, phaeanthine, is lacking. Phaeanthine is a type of benzylisoquinoline alkaloid that

## INTRODUCTION

Cancer is the second leading cause of death globally, with an approximate number of 10 million deaths in 2020 alone, and cervical cancer is the fourth most prevalent cancer worldwide, claiming one life every 2 min. It is also the leading cause of death in women cancer patients in 42 countries.<sup>1</sup> However, cervical cancer can be prevented by an early diagnosis because it takes a long time to become metastatic. Due to this reason, developing more affordable therapeutic entities can greatly help in fighting this disease.

In ancient India, traditional medicines involved ayurvedic formulations developed from plants and herbs. With advancements in technology and knowledge, these formulations have been replaced by more precise and accurate treatment strategies using bioactive molecules. So, natural products and their synthetically modified derivatives occupy a significant role in the current pharmacopeia.

For this work, we have chosen a plant that is frequently used in traditional systems but hitherto unexplored for its anticancer activity. *Cyclea peltata* (Lam) Hook.f & Thoms. belongs to the family Menispermaceae. The plant is known as Rajapata in Sanskrit and is reputedly a well-known drug quoted in most of the ancient ayurvedic classics like Charak Samhita (1000BC), Sushruta Samhita (1000BC), and Ashtangahridya (6AD). It has been widely used in many ayurvedic formulations like Pushyanuga churna for overall wellness of a women's

reproductive system and for treating many female reproductive disorders.<sup>2,3</sup> The plant enables excess water stagnation with uterine tumors, ovarian cysts, and leucorrhea to decrease.<sup>2</sup> The plant is also traditionally used by tribal communities in India to treat diarrhea, wounds, and certain skin diseases.<sup>4–6</sup> The plant is known to possess many pharmacological properties, including antidiabetic, anticancer potential at an extract level,<sup>7,8</sup> nephroprotective activity,<sup>9</sup> hepatoprotective potential,<sup>10</sup> antibacterial activity,<sup>11,12</sup> gastric antisecretory, and antiulcer property.<sup>13</sup> Additionally, *C. peltata* root extract is effective in neutralizing the venom of *Naja naja*<sup>14</sup> and also shows significant antipyretic and analgesic activity,<sup>15</sup> and the ethyl acetate extract is shown to have anti-inflammatory potential. In Swiss albino rats, the methanolic extract of the plant reduced DAL-induced tumor development.<sup>8</sup> So, based on the available literature, it is clear that the plant possesses antitumor potential, but an in-depth evaluation of the key phytomolecule, phaeanthine, is lacking. Phaeanthine is a type of benzylisoquinoline alkaloid that

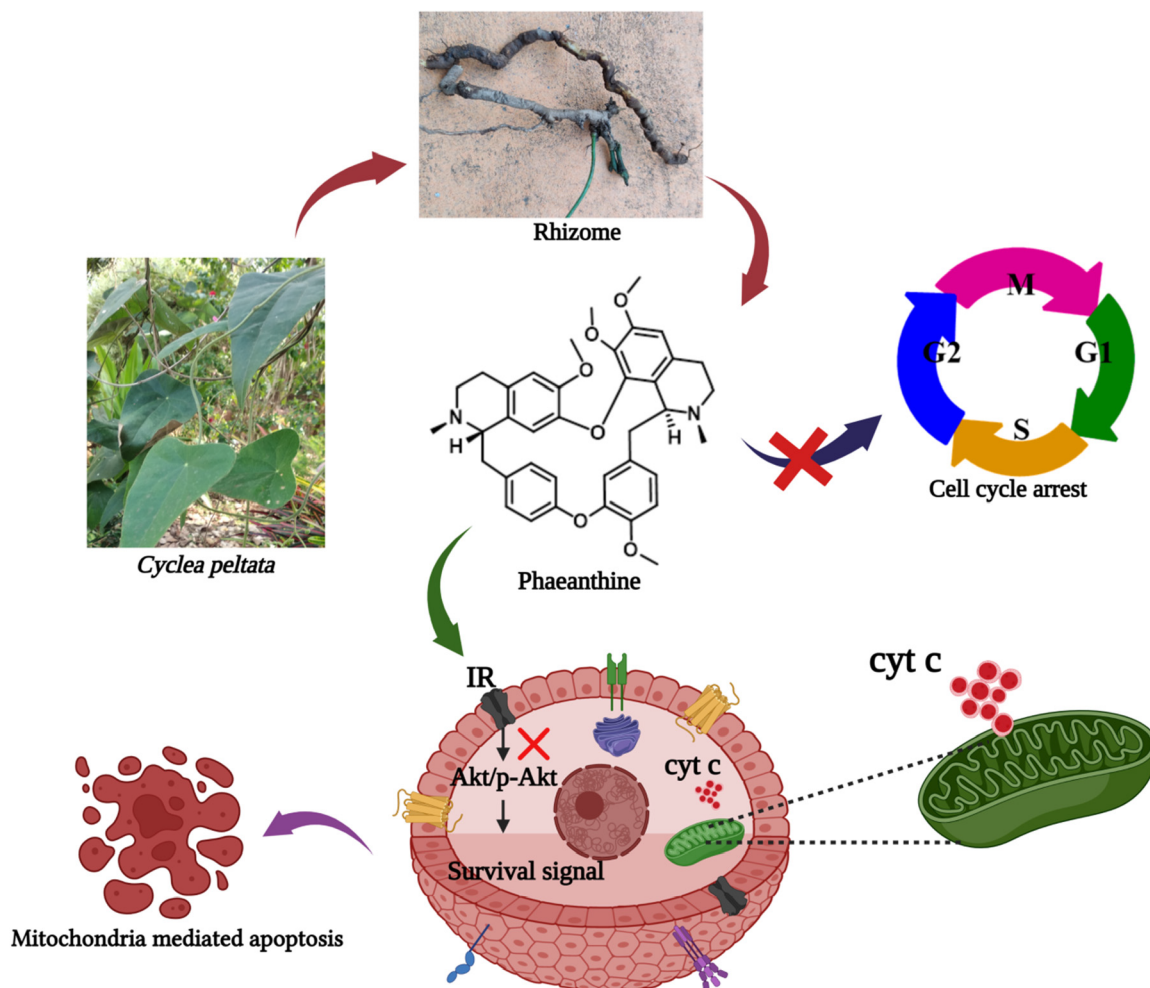
Received: February 15, 2023

Accepted: March 30, 2023

Published: April 10, 2023



## Scheme 1. Phaeanthine Downregulates Akt Signaling Pathway and Induces Mitochondria-Mediated Cell Death



includes narcotics such as codeine and morphine, muscle relaxants such as papaverine and (+)-tubocurarine, antimicrobials such as sanguinarine and berberine, and anticancer agent noscapine, among others. Phaeanthine has not been explored much in terms of its anticancer potential. Some other activities are reported for the compound, such as antiplasmodial activity,<sup>16</sup> antiprotozoal activity,<sup>17</sup> and acetylcholinesterase inhibitory potential.<sup>18</sup>

Considering the reports, we investigated the effect of phytomolecules isolated from the plant on anticancer profiling with a focus on the most common cancer of the female reproductive system, i.e., cervical cancer. We isolated the major phytomolecules from *C. peltata* rhizomes and examined the anticancer potential in the present investigation. The acetone and ethanolic extract of the plant yielded mainly three compounds, phaeanthine, cycleanine, and *N*-methylcorydaldine. Initially, all three compounds were screened for antiproliferative potential against cervical cancer cells, HeLa, among which phaeanthine was found to have appealing cytotoxicity features. In silico examination of phaeanthine demonstrated an excellent binding affinity with the proliferative protein Akt, compared to the other eight protein codes. Subsequently, the anticancer potential of phaeanthine has been evaluated with downstream in vitro assays to assess its ability to induce apoptosis, including FITC annexin V, caspase assays, and DNA fragmentation. Furthermore, clonogenic assay

and changes in mitochondrial membrane potential were also performed. As a novel insight, surface-enhanced Raman spectroscopy (SERS) was employed to scrutinize DNA fragmentation by identifying the signature Raman fingerprint of the phosphate backbone. Moreover, phaeanthine exhibited intrinsic mitochondria-mediated apoptosis and resulted in the downregulation of the expression of proliferative protein Akt and its phosphorylated form, p-Akt, and other antiapoptotic proteins Mcl-1 and XIAP (Scheme 1). To the best of our knowledge, this is the first report on the anticancer potential of phaeanthine against cervical cancer cells; HeLa cells and their apoptotic induction through mitochondria-mediated intrinsic pathway were also established.

## RESULTS AND DISCUSSION

**Extraction, Isolation, and Characterization of Phytomolecules from *Cyclea peltata* Rhizomes.** The collected *C. peltata* rhizome was subjected to sequential extraction by hexane, acetone, ethanol, and water (Figure S1). Since the acetone and ethanol extract responded to Dragendorff's test, we adopted a detailed acid–base extraction procedure. We isolated 3 compounds from the plant extract, which included 2 DBBI (dibenzylisoquinoline) alkaloids. The compounds were identified as phaeanthine (80 mg, 0.004% yield), cycleanine (50 mg, 0.0025% yield), and *N*-methylcorydaldine (30 mg, 0.0015% yield) (Figure 1) based on extensive characterization

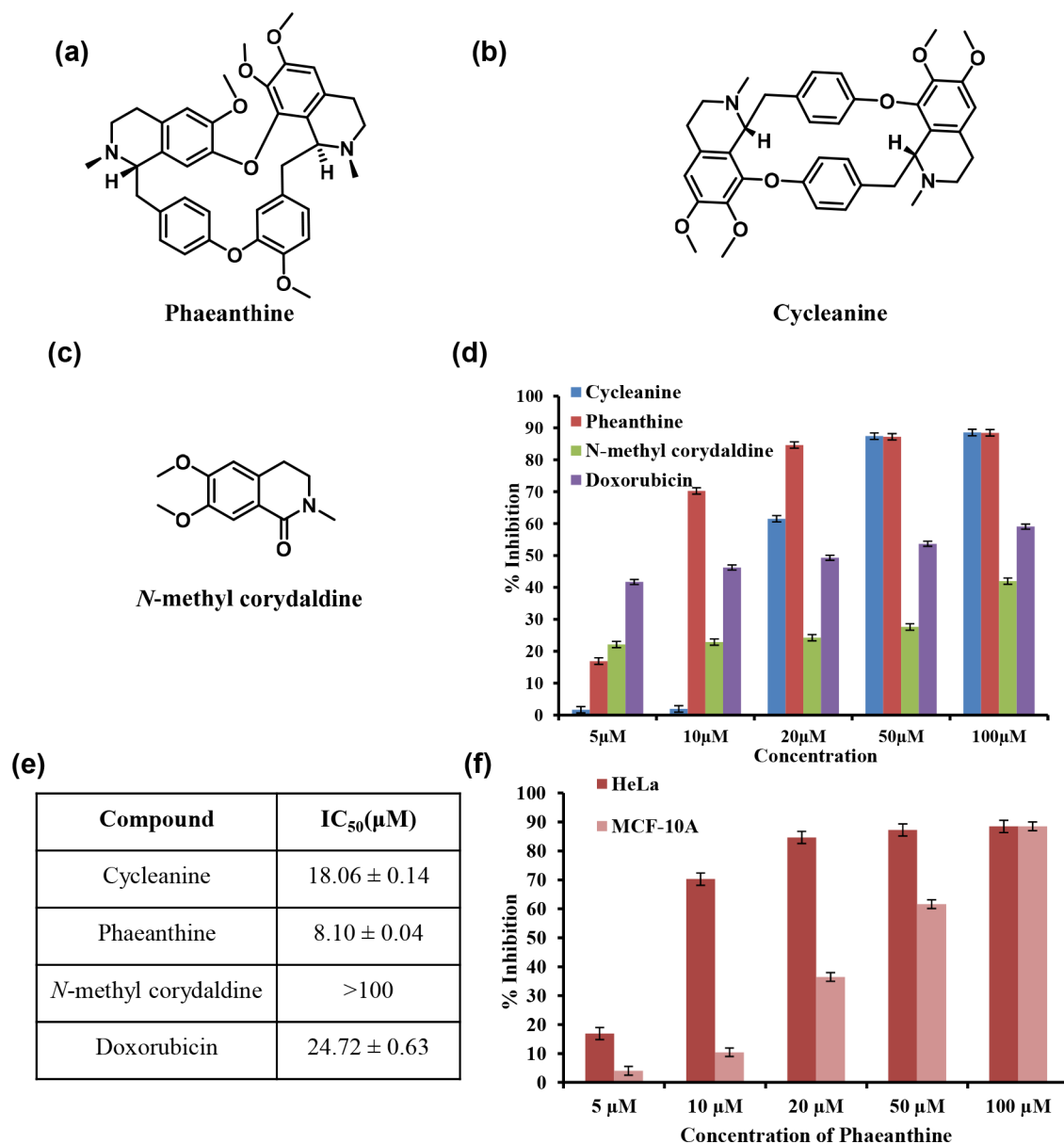


**Figure 1.** Chemical structure of the isolated compounds from *Cyclea peltata* rhizome: (a) phaeanthine, (b) cycleanine, (c) *N*-methylcorydaldine. (d) Percent inhibition on proliferation of the compounds in HeLa cells, (e) their IC<sub>50</sub> (μM) in HeLa cells for 24 h incubation, and (f) comparative % of inhibition of phaeanthine on HeLa cells and MCF-10A (nontumorigenic cell) cells for 24 h of incubation.

using the NMR technique (<sup>1</sup>H, <sup>13</sup>C, 2D) and HRMS analysis, which were in good agreement with the reported data<sup>17,19,20</sup> (Figures S2–S22).

**Primary Cytotoxicity Screening of Isolated Phytomolecules.** Preliminary selection based on the cytotoxicity of the three isolated compounds was evaluated by MTT (3-[4,5-dimethylthiazol-2-yl]-2,5-diphenyltetrazolium) assay in HeLa cells. Among the three compounds, phaeanthine showed a promising antiproliferative potential with an IC<sub>50</sub> value of 8.11 ± 0.04 μM at 24 h, whereas cycleanine showed an IC<sub>50</sub> value of 18.06 ± 0.14 μM. Although, *N*-methylcorydaldine did not show much toxicity even when concentration was increased to 100 μM (Figure 1d,e). Since phaeanthine exhibited pronounced inhibitory potential against HeLa cells at a lower concentration, we checked its toxicity against a normal nontumorigenic breast epithelial cell line, MCF-10A. To our pleasant surprise, phaeanthine did not show toxicity up to a moderate

concentration, and its IC<sub>50</sub> was found to be 36.33 ± 0.14 μM; thus the compound is not toxic up to a higher concentration. (Figure 1f). Therefore, we extended the downstream in vitro studies with phaeanthine as a potential phytomolecule.

**Computational Screening of Phaeanthine.** Next, we extended the screening strategy by employing computational tools where molecular docking was conducted with the selected proteins (Akt, MMP-2, mTOR, Survivin, caspase-9, caspase-8, p53, PARP, and STAT-3) involved in the apoptotic mechanism. Molecular docking studies among these proteins exhibited good binding affinity of phaeanthine with the target Akt, possessing a docking score of −5.023 compared to other target proteins (Table S2 and Figures S24–S32). Hence, Akt was chosen for further molecular dynamic simulation studies. In the binding interaction between Akt and phaeanthine, we observed that Thr162 donated hydrogen atoms to the ligand, leading to the formation of a H-bond with a distance of 2.31 Å. Apart from

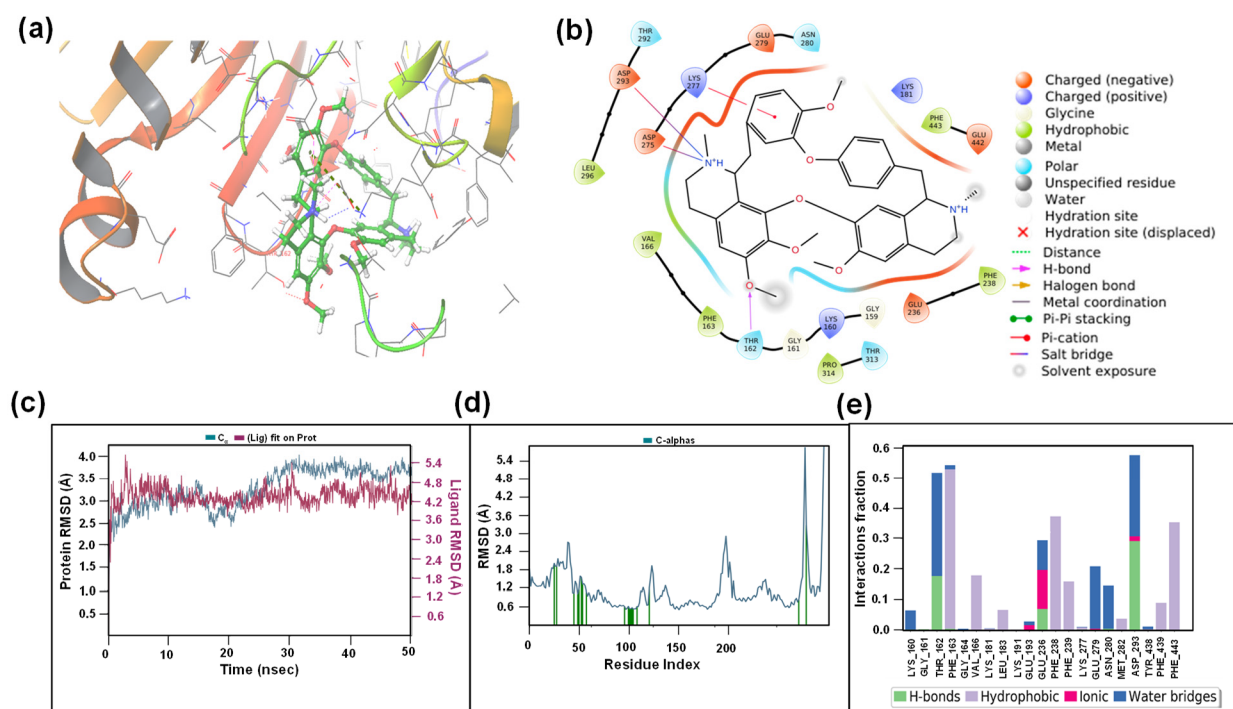


**Figure 2.** (a,b) Interaction of phaeanthine with Akt; results from MD simulation. (c) RMSD plot of Akt and phaeanthine complex; (d) RMSF plot of the protein. The green vertical line shows the residues interacting with the ligand. (e) Interactions between Akt and phaeanthine over the 50 ns simulation time.

hydrogen bonds,  $\pi$ -cation interaction and salt bridges were also observed, which may contribute to the complex's stability. The intermolecular  $\pi$ -cation interaction was formed by the interaction of a cation from Lys277 with the polarizable  $\pi$  electron cloud of an aromatic ring in phaeanthine (Figure 2a,b).

**Molecular Dynamics Simulation of Akt–Phaeanthine Complex.** To assess the stability and conformational flexibility of the Akt–phaeanthine complex, molecular dynamics simulation was performed using Desmond (academic version) of Schrödinger Suite for 50 ns under the OPLS-2005 force field. The root mean square deviation (RMSD), which gives insights into the conformational stability of the complex, was calculated throughout the 50 ns simulation time. The RMSD plot shows that the protein and protein–ligand complexes were stable until the end of the trajectory (Figure 2c). Similarly, the root mean square fluctuation (RMSF) parameter to assess flexibility was also calculated, in which minor fluctuations of the residues were found, and the residues at the N-terminal region were more fluctuated (Figure 2d). In order to further decipher the changes in the position of the ligand atoms, the ligand RMSF was calculated, which showed minor fluctuations in ligand atoms. The H-bond interactions formed by the residue Thr162 were also confirmed by protein–ligand contacts in the MD simulation (Figure 2e). The  $\pi$ -cation hydrophobic contacts which formed over the simulation time with the residues Phe163, Val166, Phe238, Phe239, Phe439, and Phe443 could also contribute to its stability. Ionic interactions, which do not involve a hydrogen bond, were also observed with the residues Glu193, Glu236, and Asp293. Apart from these interactions, water bridges involving hydrogen-bonded interactions mediated by water molecules were observed. Overall, this suggests the stability of the Akt–phaeanthine complex with the collaborative role of hydrogen bonding, hydrophobic interactions, and salt bridges.

**Apoptotic Evaluation of Phaeanthine.** First we employed a live–dead dual staining assay to differentiate the apoptotic cells where the fluorescent dyes (acridine orange and ethidium bromide) would label the viable and dead cells differently. HeLa cells were treated with phaeanthine, which showed redder to orange-colored cells than the control (green fluorescence) in a concentration-dependent manner (Figure 3a). Next, APOP staining of cells was carried out to distinguish the apoptotic cells from healthy ones, where the dead cells resembled a pink color due to membrane damage by the treatment of phaeanthine. At the same time, the untreated control did not show pink-colored cells (Figure 3b).

To corroborate the apoptosis-driven cell death by phaeanthine, we also investigated the FITC annexin V apoptosis assay. HeLa cells were treated with two different concentrations of phaeanthine (6 and 15  $\mu$ M), where the percentage of apoptotic cells showed a considerable hike in the treated cells compared to that of the control. As shown in Figure 3c, the percentage of apoptotic cells in the untreated control was 11.6%, which increased to 65.5% in cells treated with 6  $\mu$ M and 93.4% in 15  $\mu$ M phaeanthine-treated cells (Figure 3c).

**Evaluation of Caspase-Mediated Apoptosis.** Cysteine–aspartic proteases or caspases regulate the cell death pathways involving mitochondria. We have studied the expression of caspase-3, -8, and -9 by fluorometric assays. The expression of executioner caspase-3 upon treatment with phaeanthine (15  $\mu$ M) showed a hike of 2.6-fold fluorescence intensity compared to that of untreated cells. Likewise, in the case of caspase-9, cells treated with a higher concentration of compound (15  $\mu$ M) showed a similar pattern with approximately 2.3-fold increases in the fluorescence intensity compared to that with the control. But in case of caspase-8, a notable decrease in the fluorescence intensity was observed in the treated cells. At a 6  $\mu$ M concentration of phaeanthine, there was a 2.25-fold decrease,

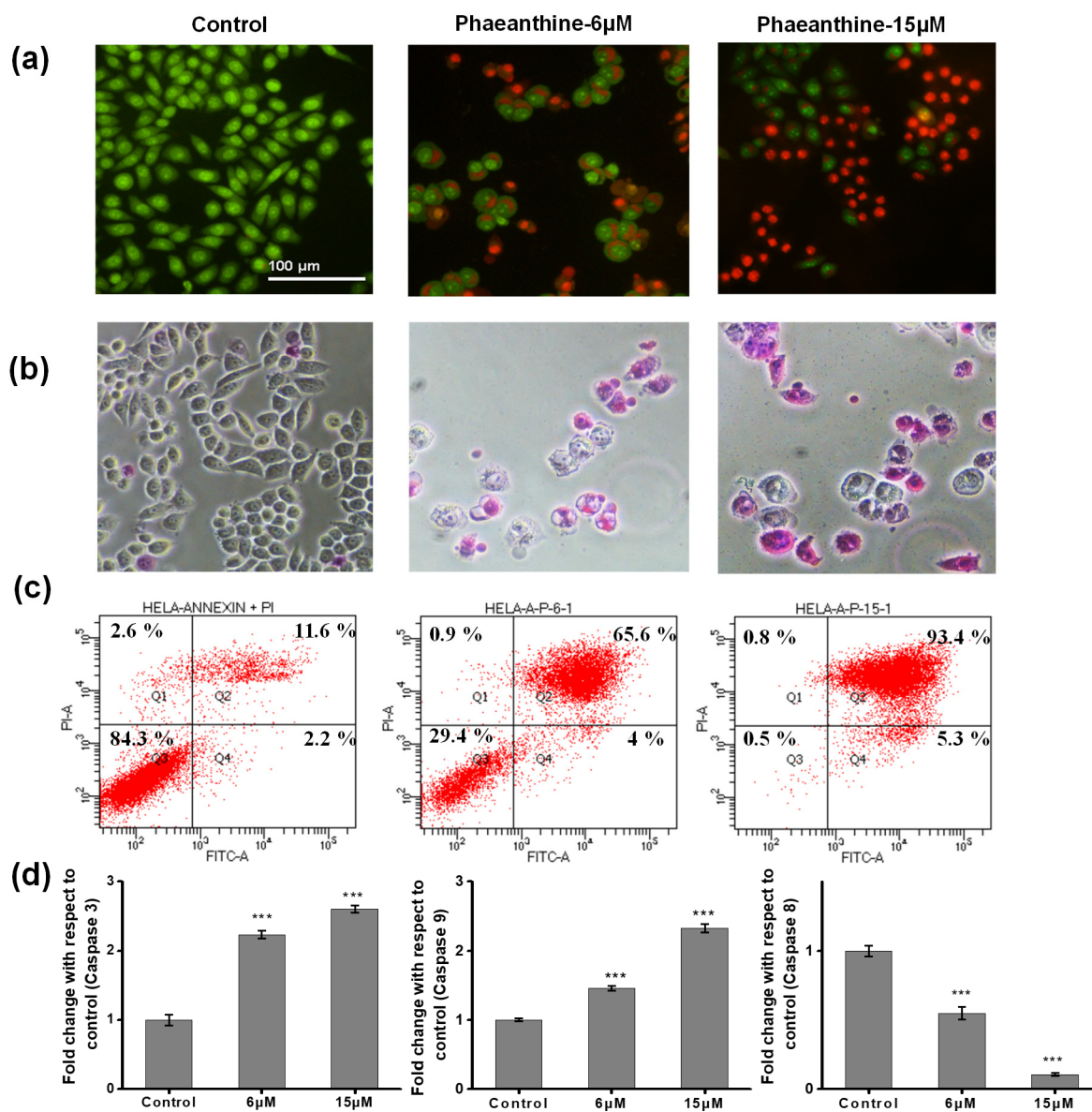


**Figure 3.** Phaeanthine-induced apoptosis in HeLa cells. HeLa cells were treated/untreated with 6 and 15  $\mu$ M concentrations for 24 h to perform (a) acridine orange–ethidium bromide dual staining assay, (b) APOP staining assay, (c) Annexin V apoptosis assay, (d) caspase fluorometric assay. The assays were carried out in triplicates, and the data are expressed as mean  $\pm$  SD; \*\*\* $p$  < 0.001, \* $p$  < 0.05 were considered to be significant as compared to the control.

and at a higher (15  $\mu$ M) concentration, a decrease in the fluorescence intensity (8.72-fold) compared to that of the control was observed (Figure 3d). The upregulation of caspase-9 and downregulation of caspase-8 substantiated the intrinsic or mitochondria-mediated apoptosis involved in the treatment of phaeanthine in HeLa cells.

**Assessment of Mitochondrial Membrane Potential Induced by Phaeanthine.** A decrease in the mitochondrial membrane potential (MMP) could be considered a marker event in the early stages of apoptosis.<sup>21</sup> JC-1 is a cationic dye that can form aggregates at a high membrane potential in the mitochondrial matrix. This polymerization will yield red emission. But in mitochondrial membrane-compromised cells or an apoptotic cell, the MMP is very low. At this low MMP, JC-1 cannot form an aggregate and will be retained as a monomer and yield green fluorescence. So, this aggregate/monomer ratio can be used as a parameter to study apoptosis in cancer cells. The

apoptotic cells will show a lower red/green or aggregate/monomer ratio. HeLa cells were treated with 5 and 8  $\mu$ M phaeanthine for 24 h of incubation, which showed a higher green fluorescence than red, indicating the JC-1 was retained as a monomer (Figure S33). The aggregate/monomer ratio is reduced compared to that of the untreated cells. The untreated cells showed an aggregate/monomer ratio of  $2.6034 \pm 0.30$ . In contrast, treated cells at 5  $\mu$ M concentration were  $0.2830 \pm 0.03$ , and at 8  $\mu$ M, phaeanthine treated cells have  $0.2013 \pm 0.05$  ratios (Figure 4a). The decrease in the aggregate/monomer ratio indicates the JC-1 aggregate formation is hindered upon the treatment by the depolymerization of membrane potential.

**Evaluation of Cytochrome *c* (cyt *c*) Dynamics by Phaeanthine.** The extent of the intrinsic apoptotic pathway was well understood by the dynamics of cyt *c*, which triggers the mitochondria-dependent apoptosis pathways. The cyt *c* is located in normal healthy cells' inner mitochondrial membrane

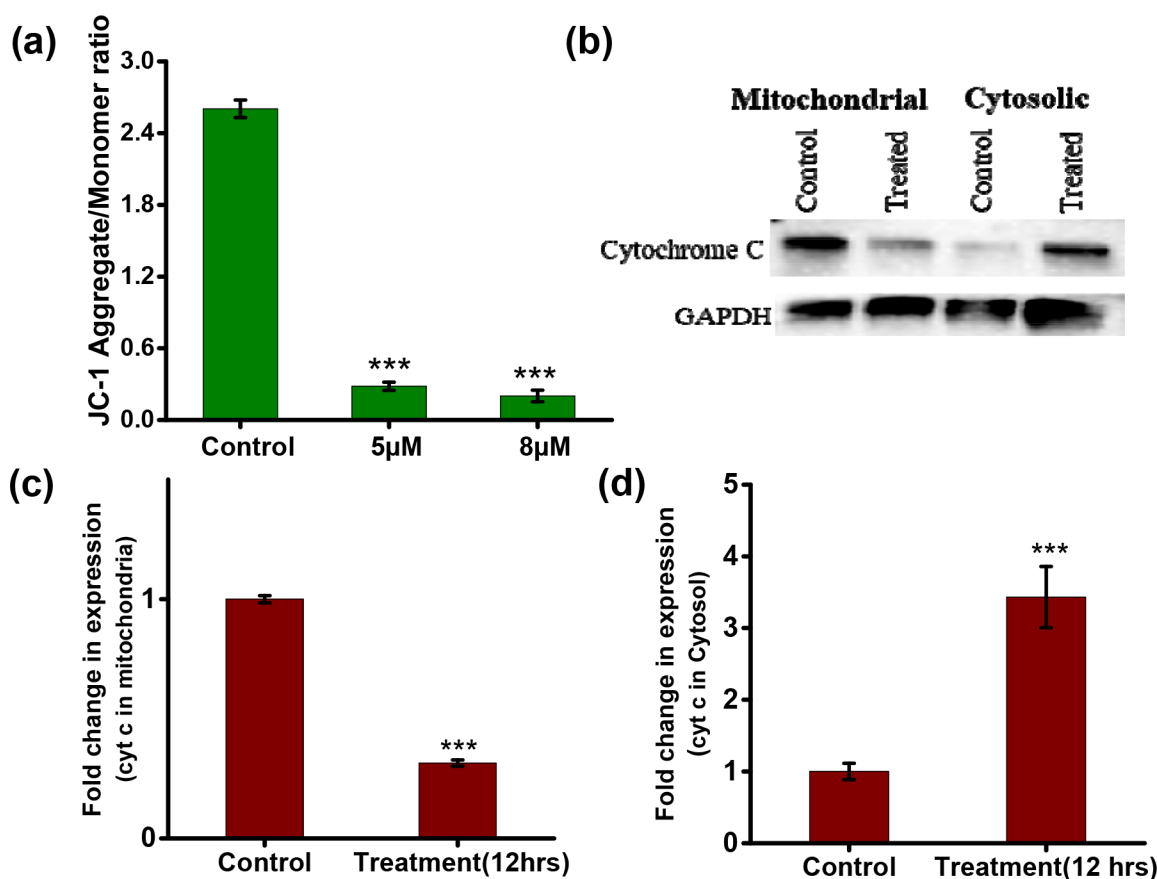


**Figure 4.** (a) Mitochondrial membrane potential evaluated by JC-1 dye: JC-1 aggregate/monomer ratio decreases with treatment at concentrations of 5 and 8  $\mu\text{M}$  phaeanthine. (b) Blot of mitochondrial and cytosolic cytochrome *c*. (c) Expression of mitochondrial cytochrome *c* in control versus phaeanthine-treated cells. (d) Expression of cytosolic cytochrome *c* in control versus phaeanthine-treated cells. The assays were carried out in triplicates, and the data are expressed as mean  $\pm$  SD; \*\*\* $p < 0.001$ , \* $p < 0.05$  were considered significant compared to the control.

space. Upon receiving apoptotic stimuli, the outer membrane gets permeabilized and releases cyt *c* to the cytosol. So, the release of cyt *c* is a noticeable change during apoptosis, or it represents mitochondria's involvement in apoptotic cell death.<sup>22</sup> We checked the expression of mitochondrial and cytosolic cyt *c* and compared their expression between phaeanthine-treated and untreated cells (Figure 4b). The results depicted the release of cyt *c* into the cytosol from mitochondria since the treated group showed an upregulation in cytosolic cyt *c* (Figure 4d). Also, downregulated mitochondrial cytochrome *c* protein expression was compared to that of the control group (Figure 4c).

**Phaeanthine-Induced DNA Condensation and DNA Fragmentation.** DNA condensation and subsequent fragmentation is a hallmark of apoptosis. Therefore, the condensation pattern of DNA was studied using a Hoechst nuclear staining assay. The nuclei of the untreated cells appeared round and uniformly stained, while the phaeanthine-treated cells showed intensely stained areas because of DNA condensation (Figure 5a).

We further carried out agarose gel electrophoresis to confirm the DNA fragmentation pattern. The isolated DNA demonstrated a laddering pattern in the cells treated with a higher concentration of phaeanthine (Figure 5b).

**Cellular Internalization and DNA Fragmentation by SERS Modality.** For further insights, we investigated Raman fingerprints of phaeanthine through surface-enhanced Raman scattering (SERS) spectral analysis (Figure 5d). Cellular

internalization of phaeanthine was tracked in a time-dependent manner in HeLa cells. Cells were treated with phaeanthine (6  $\mu\text{M}$ ) to monitor intracellular Raman fingerprints of phaeanthine with the 633 nm laser of a confocal Raman microscope using colloidal gold nanoparticles (AuNPs: 40–45 nm) as the SERS substrate. After 1 h, we observed the signature peaks of phaeanthine at 1000 and 1590  $\text{cm}^{-1}$  (aromatic ring vibrations),<sup>23,24</sup> 1160  $\text{cm}^{-1}$ , and 1212  $\text{cm}^{-1}$  (trisubstituted amine C–N stretch).<sup>25</sup> Similarly, distinct peak patterns were observed at around 2 h onward until 4 h, but after 8 h, the phaeanthine peaks decreased substantially, which may be due to its cellular metabolic decomposition.

Next, the isolated DNA from the phaeanthine-treated and the untreated cells was mixed with AuNPs, and SERS fingerprints were assessed. We identified the signature Raman peaks associated with various molecular vibrations from DNA, which were perfectly aligned with the reported literature.<sup>26,27</sup> The DNA signature peaks from 746 to 800  $\text{cm}^{-1}$ , including the ring breathing mode of pyrimidines, phosphodiester bond vibrations, especially –O–P–O stretching, as well as deoxyribose and phosphodiester bond peaks at 870 to 900  $\text{cm}^{-1}$  and aromatic ring vibrations at 1002  $\text{cm}^{-1}$  were found to be less intensified in the treated samples (Figure 5c). A similar effect was observed for 1177/1180  $\text{cm}^{-1}$  cytosine/guanine and 1303  $\text{cm}^{-1}$  adenine, cytosine peaks, and DNA mode vibrations peaks at 1573–1577  $\text{cm}^{-1}$ . We could observe enhanced peak intensity at 1620–1660  $\text{cm}^{-1}$  in higher dosage (15  $\mu\text{M}$ ) of phaeanthine-treated cellular DNA, indicating the base-pairing interactions and base-stacking

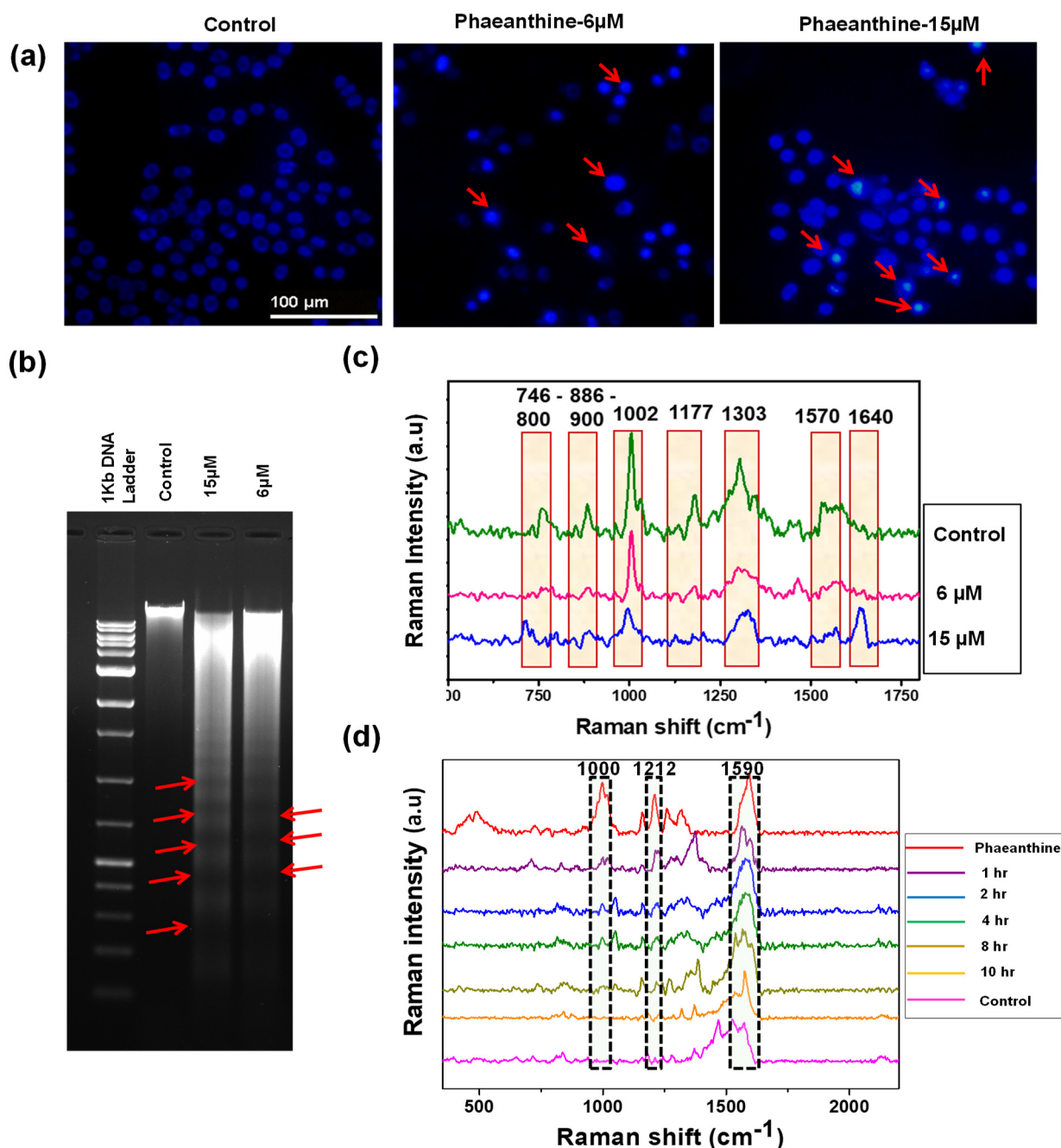


**Figure 5.** Nuclear fragmentation and condensation induced by phaeanthine: (a) Hoechst nuclear staining, (b) DNA laddering by AGE, (c) SERS analysis of DNA fragmentation, and (d) internalization of phaeanthine ( $6 \mu\text{M}$ ) into cells monitored using SERS.

effects due to H-bond formation. This may be due to DNA fragmentation associated with the base-pairing regions, leading to the generation of the particular SERS peaks in the treated sample. Thus, the SERS analysis reconfirms the apoptosis-associated DNA fragmentation in the phaeanthine treated samples.

**Inhibition of Clonogenic Potential by Phaeanthine in HeLa Cells.** Next, we investigated the inhibitory potential of phaeanthine in the colony-forming capacity of HeLa cells. The compound at  $0.5$  and  $1 \mu\text{M}$  effectively inhibited the clonogenic potential of HeLa cells. The survival fraction was substantially reduced in  $1 \mu\text{M}$  phaeanthine-treated colonies compared to that in the control colonies (Figure 6b). A very high clonogenic inhibitory potential at a significantly lower concentration ( $1$

$\mu\text{M}$ ) reflects the inhibitory ability of the compound in a dose-dependent manner (Figure 6a).

**Induction of Cell Cycle Arrest by Phaeanthine.** Flow cytometric analysis to investigate the cell cycle distribution was performed to further explore the mechanism of action of phaeanthine. Malignancies are characterized by a dysregulation of the cell cycle, which allows them to proliferate uncontrollably. Many clinically used drugs are known to induce cell cycle arrest, thereby controlling tumor growth.<sup>28</sup> We have monitored the effect of phaeanthine in regulating the cell cycle pattern upon treatment with  $6$  and  $15 \mu\text{M}$  concentrations for  $24$  h of incubation. The percentage of cells at the G1 phase decreased to  $51$  and  $41.2\%$ , respectively, compared to that of the untreated control ( $59.1\%$ ). The treated cells also showed an upsurge in the

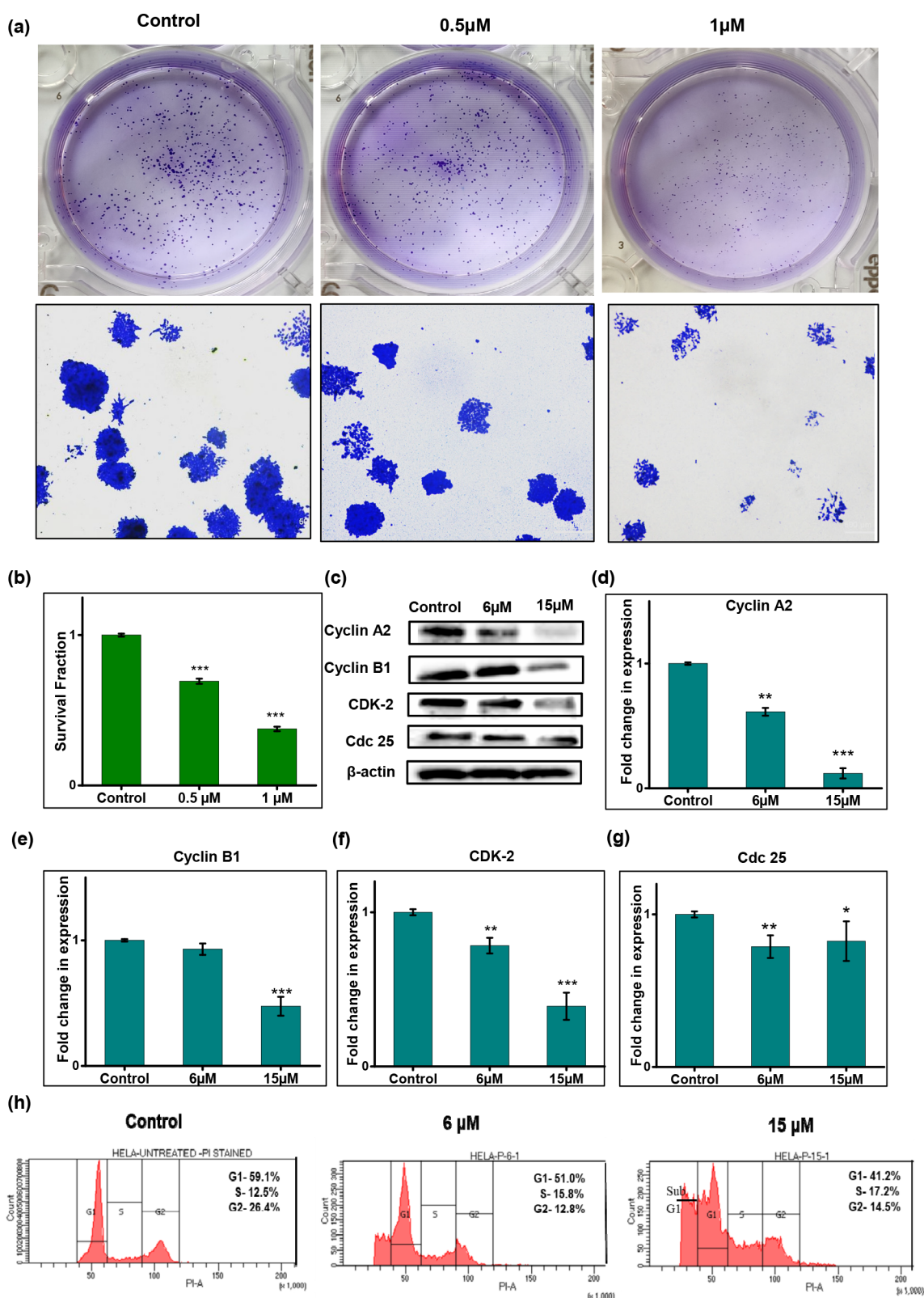


**Figure 6.** (a) Colony formation assay. (b) Survival fraction of the colonies. (c) Blot of cell cycle proteins. Expression of (d) cyclin A2, (e) cyclin B1, (f) CDK-2, and (g) Cdc 25. (h) Cell cycle assay: control denotes the untreated cells. The assays were carried out in triplicates, and the data are expressed as mean  $\pm$  SD; \*\*\* $p$  < 0.001, \*\* $p$  < 0.01, \* $p$  < 0.05 were considered to be significant as compared to the control. No asterisk (\*) represents a nonsignificant  $p$  value.

cells at the sub-G1 phase in a dose-dependent manner, indicating the apoptotic population of cells upon treatment (Figure 6h). Further, we checked the expression of some of the

key regulator proteins involved in the cell cycle regulation. Western blot analysis of various proteins such as cyclin A2, cyclin B1, CDK 2, and Cdc25c was also carried out (Figure 6c).

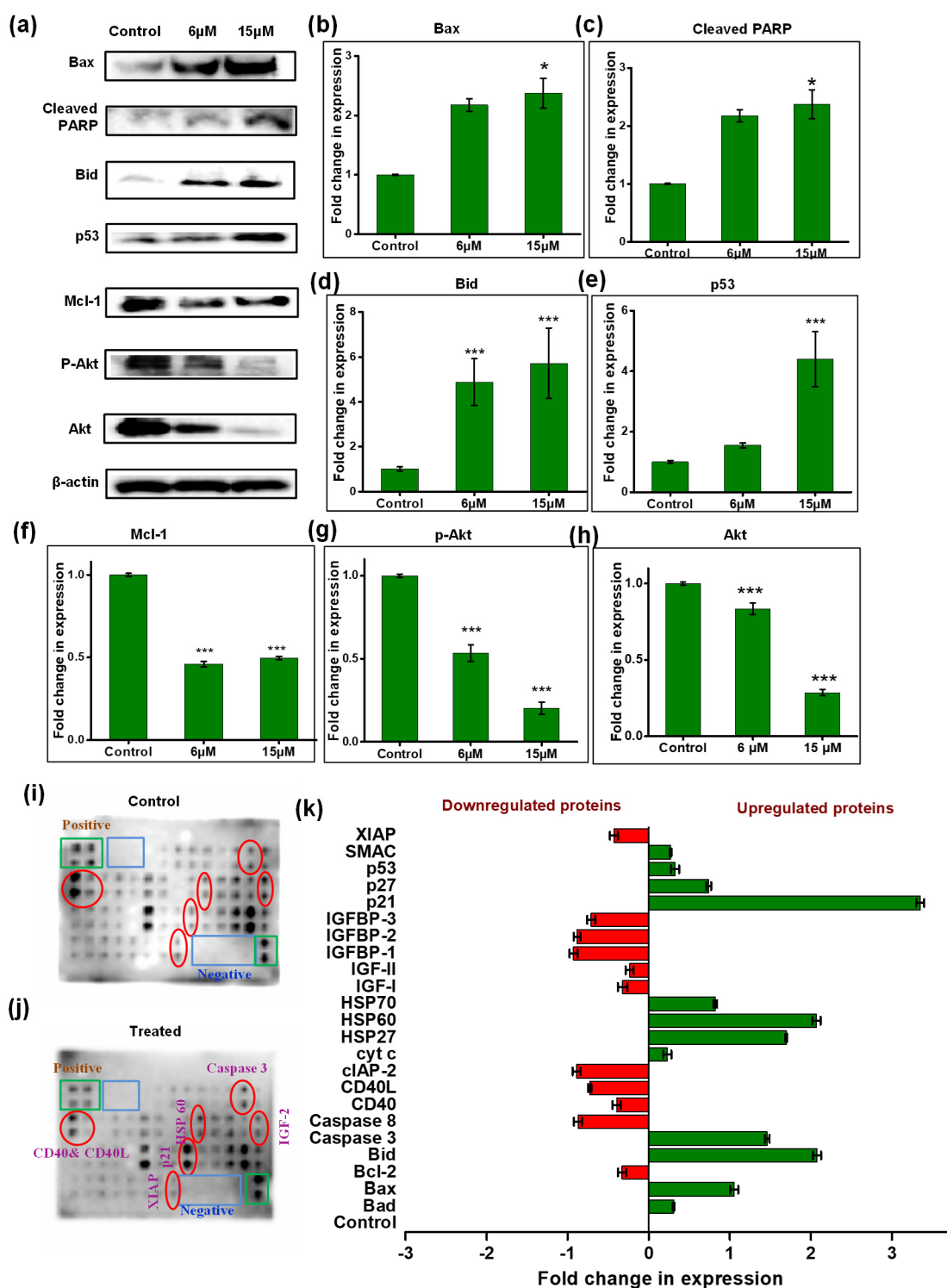


**Figure 7.** (a) Blot of apoptotic proteins. Fold change in expression of (b) Bax, (c) cleaved PARP, (d) Bid, (e) p53, (f) Mcl-1, (g) p-Akt, and (h) Akt. Apoptotic antibody array membrane analysis on HeLa cells: (i) untreated control and (j) treatment with phaeanthine at a concentration of 8  $\mu$ M for 24 h incubation and (k) fold change in expression of proteins in apoptotic array membrane treated by phaeanthine. The red color bars indicate downregulated, and the green represents upregulated proteins; the graph represents values as control intensity (1) subtracted from the normalized value of each protein. The assays were carried out in triplicates and the data are expressed as mean  $\pm$  SD; \*\*\* $p$  < 0.001, \* $p$  < 0.05 were considered significant compared to the control, and no asterisk (\*) represents a nonsignificant  $p$  value.

A significant reduction in the expression of cyclins was observed, indicating the downregulation of cell cycle proteins, thereby arresting the cell cycle to prevent the proliferation of the cancer cells. Cyclin A2 is in a strategic position to control a large part of the cell cycle because of its presence during S, G2, and

early mitosis.<sup>29</sup> Cells with repressed cyclin B1/Cdc2 activity are more likely to remain in the G2 phase, whereas cells with upregulated cyclin B1/Cdc2 activity are more likely to enter and complete mitosis.<sup>30</sup> So, the cyclin B1 downregulation will allow the cancer cells to remain in the G2 phase and arrest its entry to

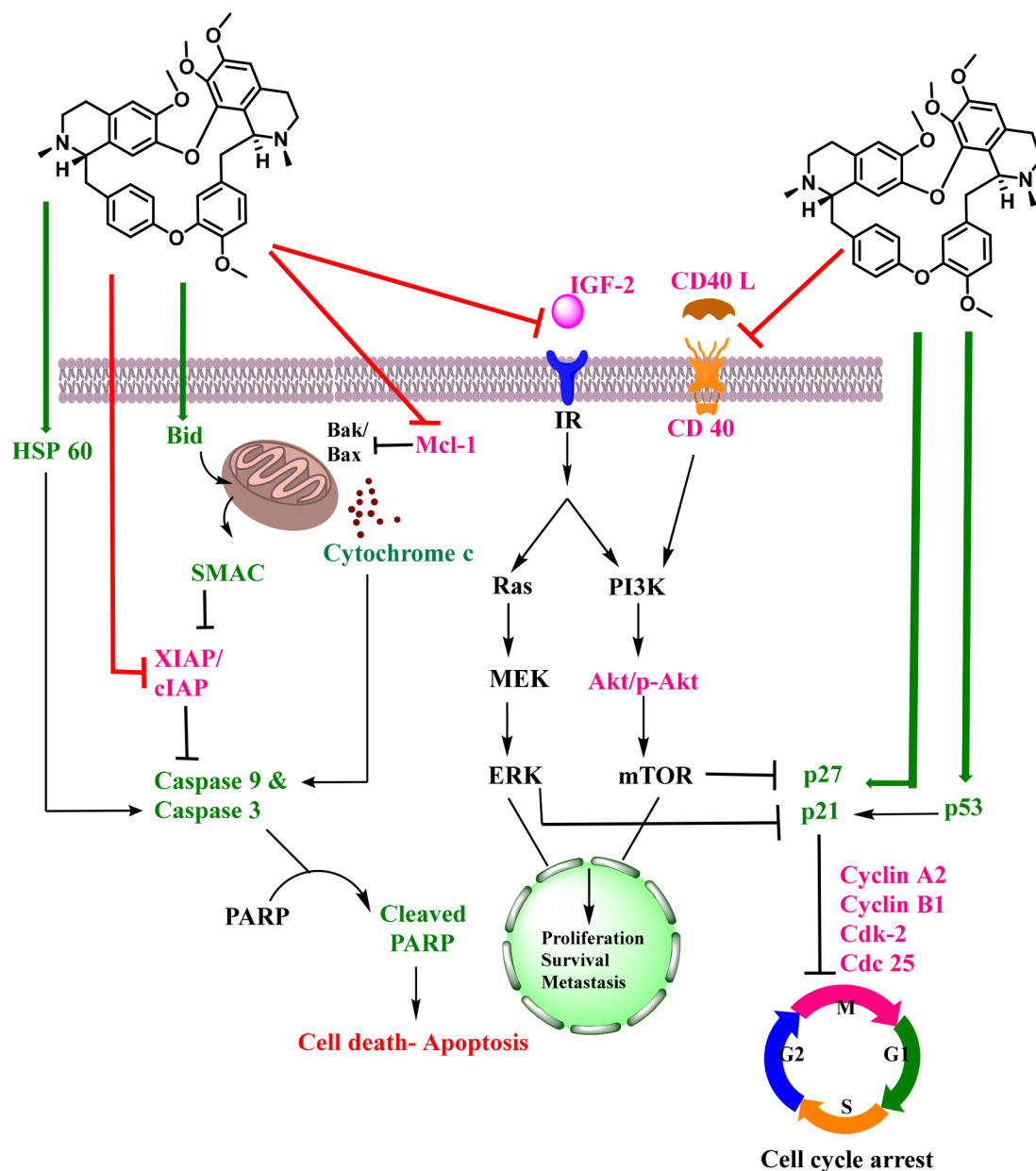


**Figure 8.** Proposed mechanism of action of phaeanthine. Red arrows indicate inhibition, and green arrows represent activation of proteins. Green colored and magenta colored entries represent experimentally validated proteins that are upregulated and downregulated, respectively, while the black colored entries are not currently evaluated.

mitosis for proliferation. CDK2 helps in the S phase to G2 phase transition by binding to cyclin E and cyclin A during the initial and terminating stages of the S phase.<sup>31</sup> Cdc25c is involved in the G2/M transition in cell cycle.<sup>32</sup> From the Western blotting of these proteins, we could observe the downregulation of all four proteins involved in the cell cycle regulation (Figure 6d–g). The results also indicate a possible chance of arrest at the G2 phase of the cell cycle, thereby regulating the proliferation of cells. Phaeanthine can control the cell cycle progression by downregulating the expression of crucial regulators such as cyclins and CDKs. Targeting cell cycle regulators always makes a better therapeutic strategy.<sup>33</sup>

**Phaeanthine-Modulated Expression of Various Proteins Involved in Apoptosis.** The promising apoptosis-inducing potential of phaeanthine encouraged us to investigate the expression of major proteins involved in the apoptotic

pathway. Western blot analysis (Figure 7a) and human apoptosis antibody array membrane assay (Figure 7i,j) were performed to evaluate the expression of key players in the apoptosis pathways. The array membrane comprises antibodies of 43 key proteins involved in the process of cell death via apoptosis. The expression studies finally revealed the alteration of various proteins. The proteins involved in promoting apoptosis, such as Bax, cleaved PARP, Bid, p53, caspase-3, p21, Hsp60, and p27, were upregulated. Treatment with phaeanthine downregulated some of the antiapoptotic proteins such as Akt, p-Akt, Mcl-1, CD40, IGF-2, and XIAP (Figure 7k). Bax and Bid are proapoptotic proteins, and the activation of caspases and p53 promotes the apoptotic pathway. High levels of IGF-2 were found to be associated with an increased risk of developing cancer.<sup>34</sup> By downregulating the expression of IGF-2, phaeanthine inhibits the binding of IGF-2 to the insulin

receptor, thereby downregulating the Ras and Akt pathway, which ultimately inhibits the survival, proliferation, invasion, and angiogenesis of cancer cells.<sup>35</sup> The regulation of Akt signaling is an important phenomenon in cancer control. We observed a downregulation in the expression of total Akt and its phosphorylated form p-Akt, thereby inhibiting PI3K/Akt signaling for survival and proliferation with phaeanthine treatment. CD40 is overexpressed in a wide variety of carcinomas; even a higher level of expression is observed in cervical carcinomas.<sup>36</sup> Activation of CD40 by CD40L results in the proliferation of cancer cells by upregulating MAPK, NF- $\kappa$ B, and JNK pathways.<sup>37</sup> So, phaeanthine-mediated downregulation of CD40 revealed an evident inhibition of the proliferative cells. X-linked inhibitor of apoptosis protein (XIAP) expression is observed to be elevated in cases of malignancies by inhibiting the activation of caspase-3 and -9 and inhibiting apoptosis-mediated cell death.<sup>38</sup> Phaeanthine induced a downregulation of XIAP, which indicates the activation of initiator and executioner caspases, thereby initiating the cellular apoptotic death mechanism. We observed a decrease in the expression of Mcl-1 protein with the treatment; Mcl-1 is usually found to inhibit the oligomerization of Bak and Bax and inhibits the release of cytochrome *c* from the mitochondrial membrane.<sup>39</sup> So, its downregulation will initiate apoptosis. Therefore, targeting Mcl-1 is a new strategy for cancer therapy.<sup>40</sup>

Bid is a proapoptotic protein which cleaves on activation and moves into the mitochondria to induce mitochondrial membrane permeabilization. This process is achieved by the oligomerization of Bax and Bak and, thus, the release of cyt *c* out of mitochondria.<sup>41</sup> Hsp60 plays a role in caspase-3 activation by functioning as a chaperone and promoting the protease-sensitive state of pro-caspase-3.<sup>42</sup> SMAC is another mitochondrial protein along with cyt *c* that gets released into the cytosol upon receiving the death signal. SMAC eradicates the action of IAPs (inhibitor of apoptosis proteins) and activates the caspase activation cascade with the help of cyt *c* and Apaf.<sup>43</sup> So, the upregulation of these proteins, namely, Bid, Hsp60, SMAC, and cyt *c*, specifies the involvement of mitochondria-mediated apoptosis in cancer cell death. Apart from these, the expression of proteins such as p21, p27, and p53 were also elevated. These proteins are involved in cell cycle arrest and regulation,<sup>44</sup> thereby controlling the tumors' further growth. From the above data, a mechanism has been proposed for cell death in HeLa cells by phaeanthine (Figure 8).

## CONCLUSION

In summary, we have successfully isolated three major alkaloids from the rhizome of *Cyclea peltata*, namely, phaeanthine, cycleanine, and *N*-methylcorydaldine. Among the three, phaeanthine showed its highest potency in inhibiting cervical cancer cell proliferation. The selected compound, phaeanthine, was found safer for the nontumorigenic cell line, MCF-10A, especially at a moderate concentration, which was adequate for apoptotic induction in HeLa cells. In silico studies of the phaeanthine revealed its good binding affinity with the antiapoptotic and proliferative protein Akt, reflecting a docking score of  $-5.023$ . The in silico data were well complemented with in vitro assessment which confirmed mitochondria-mediated apoptosis by downregulating the expression of total Akt and its phosphorylated form, p-Akt, including other antiapoptotic proteins such as Mcl-1, IGF-2, and XIAP. Furthermore, mitochondrial depolymerization and the release of cytochrome *c* into the cytosol resembled the mitochondria-mediated cell

death by the treatment of phaeanthine. As a new insight, the SERS fingerprint of phaeanthine was utilized to track cellular internalization and investigated apoptotic events by Raman fingerprint analysis of cellular DNA and other biomolecules. Finally, the phaeanthine triggered cell cycle arrest through downregulation of the expression of major regulatory proteins involved in cell cycle progression was studied, as well. To the best of our knowledge, this is the first report on the detailed in vitro anticancer studies of phaeanthine, and its inhibition on the Akt signaling pathway demonstrated in HeLa cells. These results can help in developing a better treatment strategy for cervical cancer from phaeanthine, a natural pharmacophore.

## EXPERIMENTAL SECTION

**General Experimental Procedures.** All chemicals and solvents were purchased from Sigma-Aldrich, Merck, and Spectrochem and used without further purification. Analytical TLC was performed on a Merck 60 F<sub>254</sub> silica gel plate (0.25 mm thickness), and visualization was done with UV light (254 and 365 nm). Column chromatography was performed on Merck 60 silica gel (60–120 or 100–200 mesh). The 1D and 2D NMR spectra were recorded on a Bruker ADVANCE 500 MHz, using MeOD and CDCl<sub>3</sub> as solvents, and the chemical shifts were expressed in parts per million relative to the TMS peak. The melting point was recorded on a Leica DM 2500 P optical transmission microscope equipped with a wide zoom camera and Mettler Toledo hot stage. The HRESIMS data were recorded at 60,000 resolutions using Thermo Scientific Exactive mass spectrometer. Specific rotation was measured on JASCO P-2000 polarimeter. HPLC of the compound phaeanthine was done on Shimadzu HPLC-LC 20A series (in C18 column, conditions: 0.25% acetic acid in water and methanol in the ratio 1:1, 145 kgf pressure and flow rate: 1.0 mL/min) and showed a purity of >98%.

**Extraction, Isolation, and Characterization of Phyto-molecules.** *Collection of Plant Material.* *Cyclea peltata* rhizomes were collected from Wayanad, Kerala, India. A voucher specimen of the plant was deposited in the herbarium repository of M.S. Swaminathan Research Foundation (MSSRF), Kerala, India, with voucher number M.S.S.H. 2709.

*Extraction and Isolation Procedure of C. peltata.* The rhizomes of *Cyclea peltata* were thoroughly cleaned and dried in a hot air oven maintained at 50 °C for 3 days. Approximately 2 kg of the plant material was coarsely crushed and subjected to repeated extraction using hexane, acetone, ethanol, and water, yielding 5 g of hexane extract, 20 g of acetone extract, 200 g of ethanol extract, and 10 g of water extract. Since the acetone and ethanol extract showed a positive result for Dragendorff's test for alkaloids, we adopted a detailed acid–base extraction procedure<sup>45</sup> to isolate the benzyloquinoline alkaloids from the ethanol extract, and the fractions were subjected to silica column chromatography to isolate the compounds.

**Cell Culture Methods.** The human cervical cancer cell line, HeLa, was obtained from American Type culture collection (ATCC, USA), and the normal breast epithelial cell line MCF-10A from Elabscience, USA. HeLa cells were maintained in Dulbecco's modified eagle medium (DMEM, Sigma), and MCF-10A cells were maintained in MEGM (mammary epithelial cell growth medium kit) Lonza and supplemented with 10% fetal bovine serum (FBS, Himedia) and 1% antibiotic antimycotic solution 100 $\times$  (with 10,000 units penicillin, 10 mg of streptomycin, and 25  $\mu$ g of amphotericin B per mL in 0.9%

normal saline, Himedia) and maintained at 5% CO<sub>2</sub> at 37 °C in the incubator.

**Cell Viability Assay.** Cells were seeded in a 96-well plate at a seeding density of  $8 \times 10^3$  cells/well. After 24 h of incubation, the compounds (phaeanthine, cycleanine, and *N*-methylcorydaldine) were added at different concentrations and incubated for 24 h. After incubation, the compound containing medium was removed and washed with PBS, and MTT (3-[4,5-dimethylthiazol-2-yl]-2,5-diphenyltetrazolium) at a concentration of 0.5 mg/mL was added and kept in the dark for 2–4 h. DMSO was added to dissolve the formazan crystals, and absorbance was measured at 570 nm in a multimode plate reader (Synergy H1, Biotek).

**Molecular Docking.** The X-ray crystal structure of the target proteins Akt/protein kinase B (PDB: 1O6L),<sup>46</sup> MMP-2 (1GEN), mTOR (4JSP), Survivin (1F3H), caspase-9 (2AR9), caspase-8 (4ZBW), p53 (1TUP), PARP (5DSY), and STAT-3 (6NJS) were obtained from the Protein Data Bank. The molecular docking is performed using Maestro to predict the binding modes against the active site pocket of the target protein.<sup>47</sup> Protein Preparation Wizard of the Schrödinger suite of the program is used to prepare the protein for molecular docking. Then Glide's receptor grid generation was used to generate a grid with a maximal size of  $20 \times 20 \times 20$  and 0.5 Å spacing. The molecular docking was performed using glide.<sup>48</sup>

**Molecular Dynamics Simulation.** All simulations were run with the OPLS-AA force field using the academic version of the MD simulation software, Desmond 6.9.<sup>49</sup> Desmond uses a specific neutral territory technique dubbed the midpoint approach to effectively take advantage of a high level of parallelism in the computation. We performed a 50 ns long MD simulation of the system intending to analyze the Akt aberrations in an inhibitor-bound form of phaeanthine. The system was initially set up by the system build panel and solvated in an orthorhombic box filled with water molecules. The system was then neutralized with the appropriate number of counterions and salt concentration of 0.15 M, and a 10 buffer region was allowed between the protein–ligand complex and box sides. The systems were neutralized with Na<sup>+</sup> ions, and the overlapping water molecules were deleted. The system was exposed to local energy minimization utilizing the limited memory Broyden Fletcher Goldfarb Shanno (LBFGS) algorithms and the hybrid steepest descent method. To produce simulation data for the postsimulation analyses, the system was relaxed using the constant *NPT* (number of atoms *N*, pressure *P*, and temperature *T*) ensemble condition. Using Nosé-Hoover thermostats and the Martina-Tobias-Klein barostat method, a constant temperature of 300 K and a stable atmospheric pressure of 1 atm were established for the duration of the simulation procedure. The final production MD was carried out for 50 ns for all systems, and the outcomes were examined using a simulated interaction diagram.

**Apoptotic Assays.** Various assays were used to analyze the mode of cytotoxicity induced by the compound on HeLa cells. Acridine orange–ethidium bromide dual staining and APO percentage were done to assess whether cells undergo apoptosis following the previously reported methods,<sup>50</sup> and the images were taken using a Nikon-TS100 inverted microscope. FITC Annexin V is a sensitive probe for identifying apoptotic cells, binding to the negatively charged phosphatidyl serine. It was performed with a FITC Annexin V apoptosis detection kit (BD Pharmingen, Cat. No. 556547). The kit protocol was strictly followed to conduct the experiment accurately.

**Caspase Fluorometric Assays.** The expression of various caspases upon treatment with phaeanthine was evaluated with caspase fluorometric assay kits (Biovision). The experiment was carried out as per the manufacturer's protocol. HeLa cells were treated with phaeanthine at two different concentrations (6 and 15 μM) for 24 h; after the procedures, the fluorescence intensity was measured (excitation: 400 nm and emission: 505 nm) in a multimode plate reader (Synergy H1, Biotek).

**Mitochondrial Membrane Potential Assay.** Mitochondrial membrane potential was studied using a cationic dye, JC-1 (5,5',6,6'-tetrachloro-1,1',3,3'-tetraethylimidacarbocyanine iodide) (Sigma). The cells were seeded at a density of  $7 \times 10^3$  cells/well. Phaeanthine was added at lower concentrations of 5 and 8 μM. After 24 h of incubation, cells were washed and incubated with JC-1 (5 μM) for 10 min. Cells were then observed under a Nikon-TS100 inverted microscope using red and green channel filters. The JC-1 aggregate/monomer ratio was calculated using ImageJ software.

**Cytochrome *c* Release.** Cytosolic and mitochondrial proteins of the untreated control and treated cells were isolated using a previously reported method.<sup>51</sup> Phaeanthine was added at a concentration of 6 μM and incubated for 12 h. Fractionated proteins were subjected to Western blot analysis, and mitochondrial and cytosolic cytochrome *c* expression in both control and treated sets were studied, keeping GAPDH as the internal control.<sup>52</sup> The density of each protein band was calculated using ImageJ software.

**DNA Condensation and Fragmentation Studies.** The condensation pattern of DNA induced by apoptosis was studied with Hoechst nuclear staining as previously reported.

**DNA Laddering.** HeLa cells were seeded in T75 culture flasks. The treatment was given in two different concentrations of 6 and 15 μM. The DNA was isolated using the Geneaid genomic DNA mini kit (Geneaid, cat. no. GB100), and the procedures were done per the kit protocol. The isolated DNA from treated cells and untreated control was run on 0.8% agarose gel to obtain the laddering pattern as previously reported. The image was captured with a ChemiDoc instrument (Biorad).

**Internalization and Fragmentation by SERS.** SERS fingerprinting of the isolated DNA from phaeanthine treated and untreated cells were performed by mixing the DNA with gold nanoparticles at 1:9 ratio, and a SERS spectrum was collected using a Raman spectroscope (Witek, Germany). For this, 40 nm sized gold nanoparticles were used as the SERS substrates. SERS signals were accrued using a 633 nm laser with 5 mW power and 5 s integration time. The same substrate and instrumental parameters were also employed for the phaeanthine internalization studies where the 1 mM phaeanthine in methanol was mixed with gold nanoparticles (1:9 ratio) and the SERS spectrum was collected. Further, phaeanthine-treated (6 μM) and untreated HeLa cells seeded on a chamber slide were incubated with gold nanoparticles for 10 min, and SERS analysis was performed at different time points.

**Colony Formation Assay.** First,  $1 \times 10^3$  cells/well were seeded in a 6-well plate. Compounds at two different concentrations (0.5 and 1 μM) were added after 24 h of incubation, and the cells were allowed to form colonies for the next 9 days. After that, the colonies were visualized by staining with 0.3% crystal violet for 10 min and washing with PBS.<sup>53</sup> Images were captured using a Nikon-TS100 inverted microscope and processed, and colonies were counted using ImageJ software. Survival fraction was calculated with the following formula:<sup>54</sup>

$$\text{plating efficiency (PE)} = \frac{\text{no. of colonies counted}}{\text{no. of cells seeded}} \times 100$$

$$\text{surviving fraction (SF)} = \frac{\text{PE of treated sample}}{\text{PE of control}} \times 100$$

**Cell Cycle Assay.** Cell cycle arrest induced by phaeanthine was studied using BD cycletest plus DNA kit (BD Pharmingen, cat. no. 340242). All procedures were conducted based on the kit protocol. The method involves dissolving the cell membrane lipids with a nonionic detergent, digesting cellular RNA with enzyme, and stabilizing the nuclear chromatin. PI will bind to the isolated nuclei, and the flow cytometer analyzes the light emitted by stained cells.

The expression of some of the proteins involved in the cell cycle regulation was also evaluated by Western blot. PAGE was carried out based on the standard protocol. The isolated cell lysates from phaeanthine-treated and untreated control cells were subjected to PAGE to study the expression of cyclin A2, cyclin B1, CDK-2, and Cdc 25 with their corresponding antibodies (cell signaling technology).

**Protein Expression Studies.** Cells were seeded in T75 flasks and the compound at two concentrations (6 and 15  $\mu\text{M}$ ) was added. After 24 h of incubation, cell lysate was taken according to standard procedure using RIPA buffer and protease inhibitor cocktail. BCA protein assay kit (Thermo Scientific) was used to estimate the concentration of isolated protein, and Western blotting was carried out to study the expression of various proteins. ImageJ software was used to get the band intensity of proteins. The expression of each protein was normalized with respect to the control and then with that of internal control  $\beta$ -actin.

**Apoptotic Antibody Array.** The treated and untreated cell lysate were loaded on the apoptosis antibody array membrane (Abcam, cat. no. ab134001) at equal concentrations, and all procedures were conducted based on kit protocol. The signals were detected using a chemiluminescence imaging system (BIORAD ChemiDoc). The signal intensity for each antigen-specific antibody spot is proportional to the relative concentration of the antigen (protein) in the sample. Spot signal intensities were obtained with the help of ImageJ densitometry software. The densitometric data were normalized with respect to the positive control of each membrane, and the normalization of the signals of the phaeanthine-treated lysate was done with respect to the spot on the membrane treated with lysate of untreated control cells. The relative differences in the protein expression of the treatment and control groups are obtained by comparing these signal intensities.

## ■ ASSOCIATED CONTENT

### SI Supporting Information

The Supporting Information is available free of charge at <https://pubs.acs.org/doi/10.1021/acsomega.3c01023>.

Isolation scheme, characterization of the isolated phytomolecules by NMR spectroscopic data, results of preliminary screening of the isolated compounds by MTT assay in HeLa, HPLC chromatogram of phaeanthine showing 98% purity, molecular docking data of the compound phaeanthine with various proteins and their interaction and the image of JC-1 mitochondrial membrane potential assay (PDF)

## ■ AUTHOR INFORMATION

### Corresponding Authors

**Kaustabh Kumar Maiti** – Chemical Sciences and Technology Division, CSIR-National Institute for Interdisciplinary Science and Technology (CSIR-NIIST), Thiruvananthapuram 695019, India; Academy of Scientific and Innovative Research (AcSIR), Ghaziabad 201002, India; [orcid.org/0000-0003-3368-6929](https://orcid.org/0000-0003-3368-6929); Email: [kkmaiti@niist.res.in](mailto:kkmaiti@niist.res.in)

**Kokkuvayil Vasu Radhakrishnan** – Chemical Sciences and Technology Division, CSIR-National Institute for Interdisciplinary Science and Technology (CSIR-NIIST), Thiruvananthapuram 695019, India; Academy of Scientific and Innovative Research (AcSIR), Ghaziabad 201002, India; [orcid.org/0000-0001-8909-3175](https://orcid.org/0000-0001-8909-3175); Email: [radhu2005@gmail.com](mailto:radhu2005@gmail.com)

### Authors

**Alisha Valsan** – Chemical Sciences and Technology Division, CSIR-National Institute for Interdisciplinary Science and Technology (CSIR-NIIST), Thiruvananthapuram 695019, India; Academy of Scientific and Innovative Research (AcSIR), Ghaziabad 201002, India; [orcid.org/0000-0002-8719-7138](https://orcid.org/0000-0002-8719-7138)

**Murugan Thulasi Meenu** – Chemical Sciences and Technology Division, CSIR-National Institute for Interdisciplinary Science and Technology (CSIR-NIIST), Thiruvananthapuram 695019, India; Academy of Scientific and Innovative Research (AcSIR), Ghaziabad 201002, India; [orcid.org/0000-0002-1532-496X](https://orcid.org/0000-0002-1532-496X)

**Vishnu Priya Murali** – Chemical Sciences and Technology Division, CSIR-National Institute for Interdisciplinary Science and Technology (CSIR-NIIST), Thiruvananthapuram 695019, India; [orcid.org/0000-0003-0759-991X](https://orcid.org/0000-0003-0759-991X)

**Beutline Malgija** – MCC-MRF Innovation Park, Madras Christain College, Chennai 600059, India

**Anuja Gracy Joseph** – Chemical Sciences and Technology Division, CSIR-National Institute for Interdisciplinary Science and Technology (CSIR-NIIST), Thiruvananthapuram 695019, India; Academy of Scientific and Innovative Research (AcSIR), Ghaziabad 201002, India; [orcid.org/0000-0002-7115-4889](https://orcid.org/0000-0002-7115-4889)

**Prakasan Nisha** – Academy of Scientific and Innovative Research (AcSIR), Ghaziabad 201002, India; Agroprocessing and Technology Division, CSIR-National Institute for Interdisciplinary Science and Technology (CSIR-NIIST), Thiruvananthapuram 695019, India

Complete contact information is available at:

<https://pubs.acs.org/10.1021/acsomega.3c01023>

### Author Contributions

The manuscript was written through the contributions of all authors.

### Notes

The authors declare no competing financial interest.

## ■ ACKNOWLEDGMENTS

K.K.M. thanks the Council of Scientific and Industrial Research (CSIR), Govt. of India, and Indian Council of Medical Research (ICMR), Govt. of India (No. 5/4-5/3/01/DHR/NEURO/2020-NCD-I and Accounting Code: RFC NO(P-67) NCD/Ad-hoc/220/2021-22), for research funding. AcSIR Ph.D. student A.V. (31/038(0580)/2019-EMR-I) acknowledges CSIR, New

Delhi, for financial assistance in the form of a fellowship, and M.M.T. thanks UGC for the research fellowship. V.P.M. acknowledges DHR young scientist program (R.12014/22/2021) for the funding provided. The help rendered by Mr. Vimalkumar PS for HPLC quantification is also acknowledged.

## ABBREVIATIONS

AGE, agarose gel electrophoresis; Apaf, apoptotic protease activating factor-1; Bax, BCL-2 associated X protein; Bid, BH3 interacting domain death agonist; CD40, cluster of differentiation 40; Cdc25c, cell division cycle 25c; CDK, cyclin-dependent kinases; cyt *c*, cytochrome *c*; DBBI, dibenzyl isouquinoline; DMEM, Dulbecco's modified Eagle's medium; DMSO, dimethyl sulfoxide; FBS, fetal bovine serum; FITC, fluorescein isothiocyanate; HSP60, heat shock protein 60; IC<sub>50</sub>, half-maximal inhibitory concentration; IGF-2, insulin-like growth factor-2; JNK, c-Jun N-terminal kinase; MAPK, mitogen-activated protein kinase; Mcl-1, myeloid cell leukemia-1; MEGM, mammary epithelial cell growth medium; MMP, mitochondrial membrane potential; MTT, 3-[4,5-dimethylthiazol-2-yl]-2,5-diphenyltetrazolium; NF- $\kappa$ B, nuclear factor kappa B; PAGE, polyacrylamide gel electrophoresis; PARP, poly-ADP ribose polymerase; PBS, phosphate-buffered saline; PI, propidium iodide; SERS, surface-enhanced Raman spectroscopy; SMAC, second mitochondria-derived activator of caspase; XIAP, X-linked inhibitor of apoptosis protein

## REFERENCES

- (1) UICC.org. *Cervical cancer elimination*; [https://www.uicc.org/what-we-do/thematic-areas-work/cervical-cancer-elimination#\\_ftn2](https://www.uicc.org/what-we-do/thematic-areas-work/cervical-cancer-elimination#_ftn2) (accessed 2022-08-03).
- (2) Prabha, Mukta; Akanksha Soni, K. P. A Review Article on Pushyanuga Churna in Stri Roga. *Univ. Res. Resour. J. Jayoti Vidyapeeth Women's Univ. Jaipur* **2018**, *1* (2), 71–75.
- (3) Suman Singh, K.; Nishteswar, B. R. P. A Comprehensive Review on Therapeutic Potentials of Patha (Cissampelos Pareira Linn.) from Classical Texts of Ayurveda. *Res. Rev. A J. Pharmacogn.* **2017**, 17–35.
- (4) Rajith, N. P.; Ramachandran, V. S. Ethnomedicines of Kurichyas, Kannur District, Western Ghats, Kerala. *Indian J. Nat. Prod. Resour.* **2010**, *1* (2), 249–253.
- (5) Yamuna, C. V.; Arthi, I.; Rajagopal, P. L.; Sajith Kumar, P. N.; Lithashabin, P. K.; Cyclea Peltata, A. A. K. A Pharmacological Review. *World J. Pharm. Res.* **2020**, *9* (4), 265–273.
- (6) Udhayavani, C.; Ramachandran, V. S. Knowledge and Uses of Wild Edible Plants by Paniyas and Kurumbas of Western Nilgiris, Tamil Nadu. *Indian J. Nat. Prod. Resour.* **2013**, *4* (4), 412–418.
- (7) Sangeetha, M. S.; Priyanga, S.; Hemalakshmi, S.; D, K. In Vivo Antidiabetic Potential of Cyclea Peltata in Streptozotocin Induced Diabetic Rats. *Asian J. Pharm. Clin. Res.* **2015**, *8* (1), 103108.
- (8) Meena, J. S. S. K. Efficacy of Methanolic Extract of Cyclea Peltata as a Potent Anticancer Equivalent. *Eur. J. Environ. Ecol.* **2015**, *2* (2), 65–71.
- (9) Vijayan, F. P.; Rani, V. K. J.; Vineesh, V. R.; Sudha, K. S.; Michael, M. M.; Padikkala, J. Protective Effect of Cyclea Peltata Lam on Cisplatin-Induced Nephrotoxicity and Oxidative Damage. *J. Basic Clin. Physiol. Pharmacol.* **2007**, *18* (2), 101–114.
- (10) Shine, V. J.; Latha, P. G.; Somasekharan Nair Rajam Suja, G. I.; Anuja, Raj, G.; Rajasekharan, S. N. Ameliorative Effect of Alkaloid Extract of Cyclea Peltata (P. Oir.) Hook. f. & Thoms. Roots on APAP/CCl<sub>4</sub> Induced Liver Toxicity in Wistar Rats and in Vitro Free Radical Scavenging Property. *Asian Pac. J. Trop. Biomed.* **2014**, *4* (2), 143–151.
- (11) Abraham, J.; Thomas, T. D. Antibacterial Activity of Medicinal Plant Cyclea Peltata (Lam) Hooks & Thoms. *Asian Pacific J. Trop. Dis.* **2012**, *2*, S280–S284.
- (12) Darling, R.; Raja, A.; Jeeva, S.; Prakash, J. W.; Marimuthu, J. Antibacterial Activity of Selected Ethnomedicinal Plants from South India. *Asian Pac. J. Trop. Med.* **2011**, *4* (5), 375–378.
- (13) Shine, V. J.; Latha, P. G.; Shyamal, S.; Suja, S. R.; Anuja, G. I.; Sini, S.; Pradeep, S.; Rajasekharan, S. Gastric Antisecretory and Antiulcer Activities of Cyclea Peltata (Lam.) Hook. f. & Thoms. in Rats. *J. Ethnopharmacol.* **2009**, *125*, 350–355.
- (14) Sivaraman, T.; Sreedevi, N. S.; Meenatchisundaram, S.; Vadivelan, R. Antitoxin Activity of Aqueous Extract of Cyclea Peltata Root against Naja Naja Venom. *Indian J. Pharmacol.* **2017**, *49* (4), 275–281.
- (15) Singh, S.; Nishteswar, K.; Patel, B.; Nariya, M. Comparative Antipyretic and Analgesic Activities Of Cissampelos pareira Linn. and Cyclea peltata (Lam.) Hook. F. & Thomas. *AYU (An Int. Q. J. Res. Ayurveda)* **2016**, *37* (1), 62–66.
- (16) Marshall, S. J.; Russell, P. F.; Wright, C. W.; Anderson, M. M.; Phillipson, J. D.; Kirby, G. C.; Warhurst, D. C.; Schiff, P. L. In Vitro Antiplasmodial, Antiamoebic, and Cytotoxic Activities of a Series of Bisbenzylisoquinoline Alkaloids. *Antimicrob. Agents Chemother.* **1994**, *38* (1), 96–103.
- (17) Cimanga Kanyanga, R.; Kikweta Munduku, C.; Nsaka Lumpu, S.; Tshodi Ehata, M.; Makila Bool-Miting, F.; Kambu Kabangu, O.; Mbamu Maya, B.; Cos, P.; Maes, L.; Vlietinck, A. J.; Tuentner, E.; Foubert, K.; Pieters, L. Isolation and Structure Elucidation of Two Antiprotozoal Bisbenzylisoquinoline Alkaloids from Trichlisia Gillettii Stem Bark. *Phytochem. Lett.* **2018**, *28*, 19–23.
- (18) Murebwayire, S.; Ingkaninan, K.; Changwijit, K.; Frederich, M.; Duez, P. Triclisia Sacleuxii (Pierre) Diels (Menispermaceae), a Potential Source of Acetylcholinesterase Inhibitors. *J. Pharm. Pharmacol.* **2009**, *61*, 103–107.
- (19) Scheinmann, F.; Scriven, E. F. V.; Ogbeide, O. N. Cyclicanin from Synclisia Scabrida: Conformational Information from the 1H NMR Spectrum at 300 MHz. *Phytochemistry* **1980**, *19* (8), 1837–1840.
- (20) Said, I. M.; Hamid, N. A. A.; Latif, J.; Din, L. B.; Yamin, B. M. 6,7-Dimethoxy-2-Methyl-3,4-Dihydro- Isoquinolin-1 (2H)-One. *Acta Crystallogr. Sect. E Struct. Reports* **2005**, *61*, o797–o798.
- (21) Ortega-Forte, E.; Rovira, A.; Gandioso, A.; Bonelli, J.; Bosch, M.; Ruiz, J.; Marchan, V. COUPY Coumarins as Novel Mitochondria-Targeted Photodynamic Therapy Anticancer Agents. *J. Med. Chem.* **2021**, *64*, 17209–17220.
- (22) Garrido, C.; Galluzzi, L.; Brunet, M.; Puig, P. E.; Didelot, C.; Kroemer, G. Mechanisms of Cytochrome c Release from Mitochondria. *Cell Death Differ.* **2006**, *13*, 1423–1433.
- (23) Baranska, M.; Roman, M.; Cz. Dobrowolski, J.; Schulz, H.; Baranski, R. Recent Advances in Raman Analysis of Plants: Alkaloids, Carotenoids, and Polyacetylenes. *Curr. Anal. Chem.* **2013**, *9* (1), 108–127.
- (24) Cañamares, M. V.; Pozzi, F.; Lombardi, J. R. Raman, SERS, and DFT Analysis of the Main Alkaloids Contained in Syrian Rue. *J. Phys. Chem. C* **2019**, *123*, 9262–9271.
- (25) Zhang, W.; Zhao, Y.; Bai, X.; Wang, Y.; Zhao, D. The Orientation of Protoberberine Alkaloids and Their Binding Activities to Human Serum Albumin by Surface-Enhanced Raman Scattering. *Spectrochim. Acta - Part A Mol. Biomol. Spectrosc.* **2011**, *78* (3), 1105–1109.
- (26) Movasaghi, Z.; Rehman, S.; Rehman, I. U. Raman Spectroscopy of Biological Tissues. *Appl. Spectrosc. Rev.* **2007**, *42*, 493–541.
- (27) Arya, J. S.; Joseph, M. M.; Sherin, D. R.; Nair, J. B.; Manojkumar, T. K.; Maiti, K. K. Exploring Mitochondria-Mediated Intrinsic Apoptosis by New Phytochemical Entities: An Explicit Observation of Cytochrome c Dynamics on Lung and Melanoma Cancer Cells. *J. Med. Chem.* **2019**, *62*, 8311–8329.
- (28) Diaz-moralli, S.; Tarrado-castellarnau, M.; Miranda, A.; Cascante, M. Targeting Cell Cycle Regulation in Cancer Therapy. *Pharmacol. Ther.* **2013**, *138*, 255–271.
- (29) Silva Cascales, H.; Burdova, K.; Middleton, A.; Kuzin, V.; Mullers, E.; Stoy, H.; Baranello, L.; Macurek, L.; Lindqvist, A. Cyclin A2 Localises in the Cytoplasm at the S/G2 Transition to Activate PLK1. *Life Sci. Alliances* **2021**, *4* (3), e202000980.

- (30) Choi, H. J.; Zhu, B. T. Critical Role of Cyclin B1/Cdc2 up-Regulation in the Induction of Mitotic Prometaphase Arrest in Human Breast Cancer Cells Treated with 2-Methoxyestradiol. *BBA - Mol. Cell Res.* **2012**, *1823* (8), 1306–1315.
- (31) Ding, L.; Cao, J.; Lin, W.; Chen, H.; Xiong, X.; Ao, H.; Yu, M.; Lin, J.; Cui, Q. The Roles of Cyclin-Dependent Kinases in Cell-Cycle Progression and Therapeutic Strategies in Human Breast Cancer. *Int. J. Mol. Sci.* **2020**, *21* (6), 1960.
- (32) Cho, Y.; Park, J. E.; Park, B. C.; Kim, J.; Jeong, D. G.; Park, S. G.; Cho, S. Cell Cycle-Dependent Cdc25C Phosphatase Determines Cell Survival by Regulating Apoptosis Signal-Regulating Kinase 1. *Cell Death Differ.* **2015**, *22*, 1605–1617.
- (33) Johansson, M.; Persson, J. L. Cancer Therapy: Targeting Cell Cycle Regulators. *Anticancer. Agents Med. Chem.* **2008**, *8*, 723–731.
- (34) Livingstone, C. IGF2 and Cancer. *Endocr. Relat. Cancer* **2013**, *20* (6), R321–R339.
- (35) Weroha, S. J.; Haluska, P. IGF System in Cancer. *Endocrinol. Metab. Clin. North Am.* **2012**, *41* (2), 335–350.
- (36) Eliopoulos, A. G.; Young, L. S. The Role of the CD40 Pathway in the Pathogenesis and Treatment of Cancer. *Curr. Opin. Pharmacol.* **2004**, *4* (4), 360–367.
- (37) Vonderheide, R. H. Prospect of Targeting the CD40 Pathway for Cancer Therapy. *Clin. Cancer Res.* **2007**, *13* (4), 1083–1088.
- (38) Huang, X.; Wang, X.-n.; Yuan, X.-d.; Wu, W.-y.; Lobie, P. E.; Wu, Z. XIAP Facilitates Breast and Colon Carcinoma Growth via Promotion of P62 Depletion through Ubiquitination-Dependent Proteasomal Degradation. *Oncogene* **2019**, *38* (9), 1448–1460.
- (39) Bolomsky, A.; Vogler, M.; Köse, M. C.; Heckman, C. A.; Ehx, G.; Ludwig, H.; Caers, J. MCL-1 Inhibitors, Fast-Lane Development of a New Class of Anti-Cancer Agents. *J. Hematol. Oncol.* **2020**, *13* (1), 1–19.
- (40) Wang, H.; Guo, M.; Wei, H.; Chen, Y. Targeting MCL-1 in Cancer: Current Status and Perspectives. *J. Hematol. Oncol.* **2021**, *14* (1), 1–18.
- (41) Billen, L. P.; Shamas-Din, A.; Andrews, D. W. Bid: A Bax-like BH3 Protein. *Oncogene* **2008**, *27*, S93–S104.
- (42) Xanthoudakis, S.; Sophie, R.; Rasper, D.; Hennessey, T.; Aubin, Y.; Cassidy, R.; Tawa, P.; Ruel, R.; Rosen, A.; Nicholson, D. W. Hsp60 Accelerates the Maturation of Pro-Caspase-3 by Upstream Activator Proteases during Apoptosis. *EMBO J.* **1999**, *18* (8), 2049–2056.
- (43) Du, C.; Fang, M.; Li, Y.; Li, L.; Wang, X. Smac, a Mitochondrial Protein That Promotes Cytochrome c - Dependent Caspase Activation by Eliminating IAP Inhibition. *Cell* **2000**, *102*, 33–42.
- (44) Yadav, V.; Sultana, S.; Yadav, J.; Saini, N. Gatifloxacin Induces S and G 2 -Phase Cell Cycle Arrest in Pancreatic Cancer Cells via P21/P27/P53. *PLoS One* **2012**, *7* (10), e47796.
- (45) Patel, M. B.; Mishra, S. Isoquinoline Alkaloids from *Tinospora Cordifolia* Inhibit Rat Lens Aldose Reductase. *Phyther. Res.* **2012**, *26* (9), 1342.
- (46) Yang, J.; Cron, P.; Good, V. M.; Thompson, V.; Hemmings, B. A.; Barford, D. Crystal Structure of an Activated Akt/Protein Kinase B Ternary Complex with GSK3-Peptide and AMP-PNP. *Nat. Struct. Biol.* **2002**, *9* (12), 940–944.
- (47) *Schrödinger Release 2022-2*; Maestro, Schrödinger, LLC: New York, 2022.
- (48) Friesner, R. A.; Murphy, R. B.; Repasky, M. P.; Frye, L. L.; Greenwood, J. R.; Halgren, T. A.; Sanschagrin, P. C.; Mainz, D. T. Extra Precision Glide: Docking and Scoring Incorporating a Model of Hydrophobic Enclosure for Protein-Ligand Complexes. *J. Med. Chem.* **2006**, *49* (21), 6177–6196.
- (49) *Maestro-Desmond Interoperability Tools*, Schrödinger; D. E. Shaw Research: New York, 2021.
- (50) Joseph, M. M.; Aravind, S. R.; George, S. K.; Pillai, K. R.; Mini, S.; Sreelekha, T. T. Galactoxyloglucan-Modified Nanocarriers of Doxorubicin for Improved Tumor-Targeted Drug Delivery with Minimal Toxicity. *J. Biomed. Nanotechnol.* **2014**, *10* (11), 3253–3268.
- (51) Dimauro, I.; Pearson, T.; Caporossi, D.; Jackson, M. J. A Simple Protocol for the Subcellular Fractionation of Skeletal Muscle Cells and Tissue. *BMC Res. Notes* **2012**, *5* (1), 513.
- (52) Lu, X.; Costantini, T.; Lopez, N. E.; Wolf, P. L.; Hageny, A. M.; Putnam, J.; Eliceiri, B.; Coimbra, R. Vagal Nerve Stimulation Protects Cardiac Injury by Attenuating Mitochondrial Dysfunction in a Murine Burn Injury Model. *J. Cell. Mol. Med.* **2013**, *17* (5), 664–671.
- (53) Aswathy, M.; Banik, K.; Parama, D.; Sasikumar, P.; Harsha, C.; Joseph, A. G.; Sherin, D. R.; Thanathu, M. K.; Kunnumakkara, A. B.; Vasu, R. K. Exploring the Cytotoxic Effects of the Extracts and Bioactive Triterpenoids from *Dillenia Indica* against Oral Squamous Cell Carcinoma: A Scientific Interpretation and Validation of Indigenous Knowledge. *ACS Pharmacol. Transl. Sci.* **2021**, *4* (2), 834–847.
- (54) Franken, N. A. P.; Rodermond, H. M.; Stap, J.; Haveman, J.; van Bree, C. Clonogenic Assay of Cells in Vitro. *Nat. Protoc.* **2006**, *1* (5), 2315–2319.